Photomediated Oxidation of Atomically Precise Au 25 (SC 2 H 4 Ph) 18 – Nanoclusters

ARTICLE *in* JOURNAL OF PHYSICAL CHEMISTRY LETTERS · JANUARY 2013

Impact Factor: 7.46 · DOI: 10.1021/jz302056q

5 AUTHORS, INCLUDING:

Gao Li
Dalian Institute of Chemical Physics
47 PUBLICATIONS **1,215** CITATIONS

SEE PROFILE

THE JOURNAL OF PHYSICAL CHEMISTRY Letters

Letter

pubs.acs.org/JPCL

Photomediated Oxidation of Atomically Precise $Au_{25}(SC_2H_4Ph)_{18}^-$ Nanoclusters

Douglas R. Kauffman,*[,†,‡] Dominic Alfonso,[†] Christopher Matranga,[†] Gao Li,[§] and Rongchao Jin[§]

[†]National Energy Technology Laboratory (NETL), United States Department of Energy, Pittsburgh, Pennsylvania 15236, United States

[‡]URS, P.O. Box 618, South Park, Pennsylvania 15129, United States

[§]Department of Chemistry, Carnegie Mellon University, Pittsburgh, Pennsylvania 15213, United States

Supporting Information

ABSTRACT: The anionic charge of atomically precise $Au_{25}(SC_2H_4Ph)_{18}^-$ nanoclusters (abbreviated as Au_{25}^-) is thought to facilitate the adsorption and activation of molecular species. We used optical spectroscopy, nonaqueous electrochemistry, and density functional theory to study the interaction between Au_{25}^- and O_2. Surprisingly, the oxidation of Au_{25}^- by O_2 was not a spontaneous process. Rather, Au_{25}^-–O_2 charge transfer was found to be a photomediated process dependent on the relative energies of the Au_{25}^- LUMO and the O_2 electron-accepting level. Photomediated charge transfer was not restricted to one particular electron accepting molecule or solvent system, and this phenomenon likely extends to other Au_{25}^-–adsorbate systems with appropriate electron donor–acceptor energy levels. These findings underscore the significant and sometimes overlooked way that photophysical processes can influence the chemistry of ligand-protected clusters. In a broader sense, the identification of photochemical pathways may help develop new cluster-adsorbate models and expand the range of catalytic reactions available to these materials.

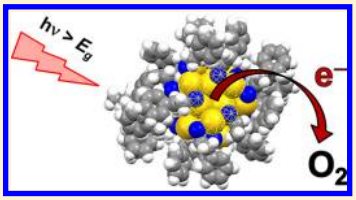

SECTION: Physical Processes in Nanomaterials and Nanostructures

Atomically precise, ligand-protected $Au_{25}(SC_2H_4Ph)_{18}^-$ clusters (abbreviated as Au_{25}^-) are a fascinating class of nanomaterials because they bridge the size-gap between molecules and traditional nanoparticles, they have a precisely known surface structure, and they possess an inherent negative charge.[1,2] Au_{25}^- also differs from traditional nanoparticles because quantum confinement leads to significant energy level quantization and the development of a molecule-like electronic structure.[3−5] These characteristics make Au_{25}^- a unique system for studying molecular adsorption and chemical reactions.

Ligand-protected Au_{25}^- clusters have shown exceptional catalytic activity and product selectivity for the oxidation of styrene[6] and CO,[7] the hydrogenation of ketones and aldehydes,[6,8,9] and the electrochemical reduction of CO_2[10] and O_2.[11] The cluster's inherent negative charge is thought to facilitate the adsorption and activation of various molecules, and this hypothesis has been a central feature in mechanistic descriptions of Au_{25}^- reactivity.[6−10,12] In general, computational models have had difficulty capturing the apparent catalytic activity of ligand-protected Au_{25}^-, and studies often require the partial or complete removal of ligand groups to promote molecular adsorption and chemical reactions.[13−15] Removing ligands from such small clusters will significantly impact their electronic structure,[13] and the resulting computational models or experimental samples[16,17] will differ from the ligand-protected clusters most often used in experiments. The discrepancy between the experimentally observed and computationally predicted reactivity of ligand-protected clusters illustrates a gap in our understanding of Au_{25}^- chemistry, and the precise reaction sites, the role of ligands, and the associated reaction pathways are not well-defined in the literature. As such, new experimental and computational studies aimed at probing realistic cluster models are needed to advance the field.

O_2 was used as a molecular probe to study the surface chemistry of Au_{25}^-. Not only is O_2 a prototypical electron-accepting molecule, but understanding O_2 adsorption and charge-transfer processes is fundamentally important for catalytic oxidation reactions and fuel cell applications. A combination of optical spectroscopy, nonaqueous electrochemistry, and density functional theory (DFT) was used to investigate the interaction between Au_{25}^- and O_2. The DFT calculations specifically considered *fully* ligand-protected Au_{25}^- clusters to address the binding sites and energetics associated with O_2 adsorption.

We show that typical room light can have an unexpectedly large impact on Au_{25}^- chemistry. Our results reveal that the cluster's negative charge contributes very little (if at all) to its ground-state interaction with O_2. Rather, we found that ambient room light photoexcited the Au_{25}^- cluster and promoted photomediated charge transfer. This phenomenon was not restricted to one particular electron accepting molecule or solvent system, and it is likely a general chemical process for Au_{25}^-–adsorbate systems with appropriate electron donor–

Received: December 12, 2012
Accepted: December 19, 2012
Published: December 19, 2012

acceptor energy levels. These findings illustrate the important but sometimes overlooked role that photophysical processes can have on the chemistry of ligand-protected clusters. In fact, significant chemical insight can be gained from simple reactions like Au_{25}^- oxidation by O_2 when photoaccessible charge-transfer pathways are considered. In a broader sense, these findings have practical implications for the synthesis, handling, and study of ligand-protected metal clusters in typical, well-lit laboratory settings.

The Au_{25}^- crystal structure has been theoretically predicted[18] and experimentally solved.[1,2] The cluster contains a Au_{13} core within a shell of six −S−Au−S−Au−S− semiring structures (Figure 1a). This atomic arrangement provides Au_{25}^- with unique stability, and its structure persists even after chemical treatment with $Ce(SO)_4$, H_2O_2, or $NaBH_4$,[12,19,20] ligand exchange,[21] or the application of electrochemical potentials.[10] The stability of the Au_{25}^- structure is quite remarkable considering that thiolate monolayers (ligands) can desorb from traditional Au surfaces under much milder conditions.[22]

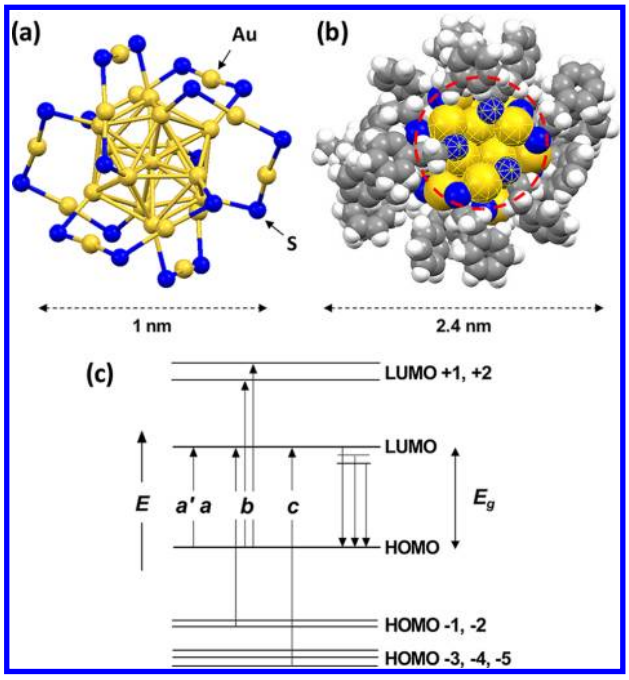

Figure 1. (a) Structure of the $Au_{25}(SC_2H_4Ph)_{18}^-$ cluster (abbreviated as Au_{25}^-) shown here without the organic ligands to emphasize the Au_{13} core and the six −S−Au−S−Au−S− semirings in the shell.[1,2] (b) Space-filled model of the Au_{25}^- cluster with the $-C_2H_4Ph$ organic ligands; the proposed active site is circled and red and the individual atoms are highlighted with yellow crosshatches. The anionic cluster is accompanied by a tetraoctylammonium counterion (TOA^+) and the Au_{25}^-−TOA^+ couple is presented in Figure S1 in the Supporting Information. The cluster structures were created using the crystallographic information files published in refs 1 and 2. (c) Simplified Au_{25}^- energy level diagram that was created from the data in ref 1. The electronic transitions correspond to the labeled absorbance peaks in Figure 2a.

Figure 1b presents a space-filled model of the Au_{25}^- cluster including the organic $-C_2H_4Ph$ ligands. The ligand orientation leaves an accessible surface site on the Au_{25}^- cluster that has been identified in the adsorption of a variety of molecular species.[8−10,23] The active site is composed of a "pocket" of three core Au atoms, three shell Au atoms, and three shell S atoms; the general area of the adsorption site is circled in red, and the specific atoms are highlighted with yellow cross-hatches. The anionic cluster is accompanied by a single tetraoctylammonium counterion (TOA^+), and the Au_{25}^-−TOA^+ couple is shown in Figure S1 in the Supporting Information.

The quantum confinement of electrons within the small cluster leads to significant energy level quantization and the development of several molecule-like optical transitions. Figure 1c presents a simplified energy level diagram for Au_{25}^- (ref 1). The *a*′ and *a* transitions represent the photoexcitation of Au_{25}^- electrons from the HOMO into the LUMO with a computationally predicted energy gap (E_g) of 1.37 eV.[1] Experimentally, the Au_{25}^- absorbance onset occurred at 1.36 eV (Figure S2 in the Supporting Information), and splitting of the degenerate HOMO separated and blue-shifted the *a*′ and *a* transitions.[24−26] Transition *b* corresponds to HOMO−2 → LUMO and HOMO → LUMO+1,+2 photoexcitations, and transition *c* represents a HOMO−5 → LUMO photoexcitation.[1] Au_{25}^- also demonstrates a broad photoluminescence (PL) profile that stems from the relaxation of photoexcited electrons into emissive midgap states.[27]

Figure 2a contains the optical absorbance and PL spectra of Au_{25}^- dissolved in dimethylformamide (DMF); the labeled absorbance peaks correspond to the transitions defined in Figure 1c. The black curves in Figure 2a represent the absorbance and PL spectra of an initially N_2 purged Au_{25}^-

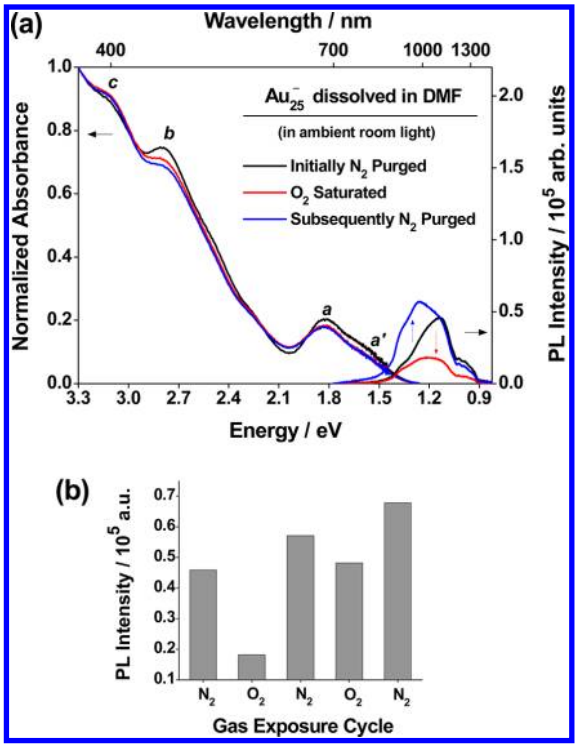

Figure 2. Spectroscopic response of Au_{25}^- to O_2 in ambient room light. (a) Absorbance and photoluminescence (PL) spectra of Au_{25}^- in DMF that was initially purged with N_2 (black curves), saturated with O_2 in ambient room light (red curves), and subsequently purged with N_2 (blue curves). The absorbance spectra were normalized at 3.3 eV to standardize the spectral background, and the raw absorbance spectra are plotted in Figure S3 in the Supporting Information for comparison. (b) PL intensity of Au_{25}^- in DMF that was repeatedly purged with N_2 and saturated with O_2 in ambient room light; 1 h N_2 and O_2 gas exposure cycles.

dx.doi.org/10.1021/jz302056q | J. Phys. Chem. Lett. 2013, 4, 195−202

solution; the absorbance spectra were normalized at 3.3 eV to standardize the background, and the raw spectra are plotted in Figure S3 in the Supporting Information for comparison. The PL spectra in Figure 2a were collected with a liquid N_2-cooled InGaAs detector, and they are consistent with other reports of near-infrared (NIR) LUMO→HOMO photoemission.[27−29] Some researchers have reported higher energy PL that likely originates from states above the Au_{25}^- LUMO.[21,30−33] The detectors used in these reports were not necessarily optimized for the NIR spectral region, and the reported PL maxima typically contained energy greater than the Au_{25}^- E_g.

Au_{25}^- is sensitive to the local chemical environment, and charge transfer or charge rearrangement will impact the absorbance and PL spectra in characteristic ways. The red curves in Figure 2a represent the Au_{25}^- solution after it was bubbled with O_2 for 1 h in ambient room light; this O_2 exposure time was chosen to ensure solution saturation. Depopulation of the Au_{25}^- HOMO partially bleached the *a*, *a*′, and *b* absorbance peaks, and an oxidation-based change in cluster geometry increased the peak area of transition *c* and the absorbance at 2.04 eV.[12] These changes were reproducible from sample to sample (Table S1 in the Supporting Information), and they were consistent with previous examples of Au_{25}^- oxidation with O_2,[12,30] dissolved cations,[29,34,35] peroxide species,[36] or electrochemical potentials.[27]

The PL intensity of O_2-saturated Au_{25}^- solutions was decreased by 52 ± 8% and blue-shifted by 131 ± 8 meV (red curve; Figure 2a). On the outset, this result was unexpected because oxidation tends to increase the Au_{25}^- PL,[10,28−30] but after O_2 was purged from the solution, the PL intensity increased 25 ± 1% beyond its initial value (blue curve, Figure 2a). This reversible quenching phenomenon allowed modulation of the Au_{25}^- PL intensity through repeated N_2 purging and O_2 saturation cycles (Figure 2b). However, the PL intensity gradually increased over subsequent N_2/O_2 cycles due to apparent cluster oxidation. The origins of the oxidation-based PL increase and blue shift are still unresolved, but oxidation slightly changes the cluster geometry[12] and may further polarize Au−S bonds in the cluster shell.[28,30] We hypothesize that either phenomena could increase and blue shift PL through a reduction in nonradiative relaxation pathways.

Interestingly, oxidation-like spectral changes were *not* found after light-free O_2 exposures, although solvent evaporation did cause a small 10 ± 1% increase and 5 ± 3 meV blue shift in the Au_{25}^- PL (Figures S4 and S5 in the Supporting Information). To further explore this apparent photomediated interaction, we used a fiber optic light source and a series of band-pass and low-pass optical filters to illuminate O_2 saturated Au_{25}^- solutions (see methods section and Figures S6 and S7 in the Supporting Information). This approach allowed us to isolate the sample from ambient light and selectively illuminate solutions with light corresponding to particular Au_{25}^- optical transitions. We found equivalent spectral changes after O_2-saturated solutions were illuminated with light corresponding to any single peak or combination of peaks within the Au_{25}^- absorbance spectrum (Figures S8−S12 in the Supporting Information). However, these changes did *not* occur if the light contained less energy than the Au_{25}^- HOMO−LUMO gap energy (Figure S13 in the Supporting Information).

Figure 3 and Table S1 in the Supporting Information summarize the Au_{25}^- spectral changes following O_2 exposure in the dark, under ambient room light, and under illumination

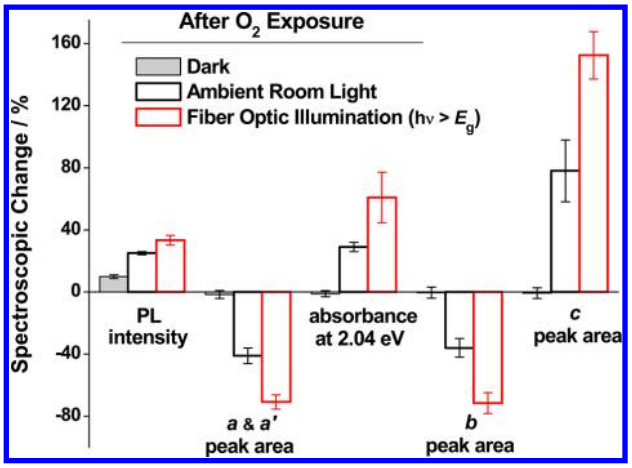

Figure 3. Spectroscopic changes after Au_{25}^- solutions (in DMF) were bubbled with O_2 for 1 h and then purged with N_2. Fiber optic illumination was conducted through various band-pass and low-pass optical filters; in all cases the filtered light contained energy greater than the Au_{25}^- HOMO−LUMO gap (Figures S8−S12 in the Supporting Information). The error bars are from three to five runs with freshly prepared Au_{25}^- solutions, and the data are summarized in Table S1 in the Supporting Information. A 10 ± 1% PL increase in the dark stemmed from solvent evaporation during gas bubbling—this occurred even if the solution was exclusively bubbled with N_2 (Figures S4 and S5 in the Supporting Information).

with a fiber optic light source; these changes were measured after the solution was bubbled with O_2 for 1 h and then purged with N_2. The small PL increase after dark O_2 exposure stemmed from solvent evaporation (Figures S4 and S5 in the Supporting Information). The higher intensity fiber optic source generally produced larger spectral changes compared with ambient room light, but equivalent PL blue shifts were found after room light and fiber optic illumination. Similar photomediated Au_{25}^-−O_2 charge transfer occurred in *p*-xylene (Figure S14 in the Supporting Information), indicating that this phenomenon is not restricted to one particular solvent.

DFT calculations were carried out to model O_2 adsorption on a fully ligand-protected $Au_{25}(SCH_3)_{18}^-$ cluster (Figure 4). These computations are a valuable addition to experimental techniques because they provide atomic-level descriptions of surface processes. We identified two weakly bound states between O_2 and the $Au_{25}(SCH_3)_{18}^-$ active site. O_2 was found to bind to three shell S atoms or one shell Au atom within the adsorption pocket. Figure 4a,c presents ball and stick models of the O_2 adsorption configurations. The accompanying space-filled models (Figure 4b,d) emphasize the position and orientation of the of O_2 molecule with respect to the $Au_{25}(SCH_3)_{18}^-$ active site. In both cases, O_2 binding energies were smaller than −0.2 eV (negative binding energies are considered stable), the calculated S−O and Au−O bond distances ranged between 3.4 and 3.5 Å, and the calculated O−O bond distance of adsorbed O_2 (1.25 Å) was essentially the same as free O_2 (1.24 Å).[13]

The prediction of weak binding between fully ligand-protected, ground-state $Au_{25}(SCH_3)_{18}^-$ and O_2 is quite important because it suggests that spontaneous Au_{25}^-−O_2 charge transfer is unlikely. These results support our hypothesis that Au_{25}^-−O_2 charge transfer is a photomediated process, and they are consistent with the lack of Au_{25}^- spectral changes during light-free O_2 exposure. In comparison, Häkkinen and coworkers theoretically studied strongly bound states between

dx.doi.org/10.1021/jz302056q | J. Phys. Chem. Lett. 2013, 4, 195−202

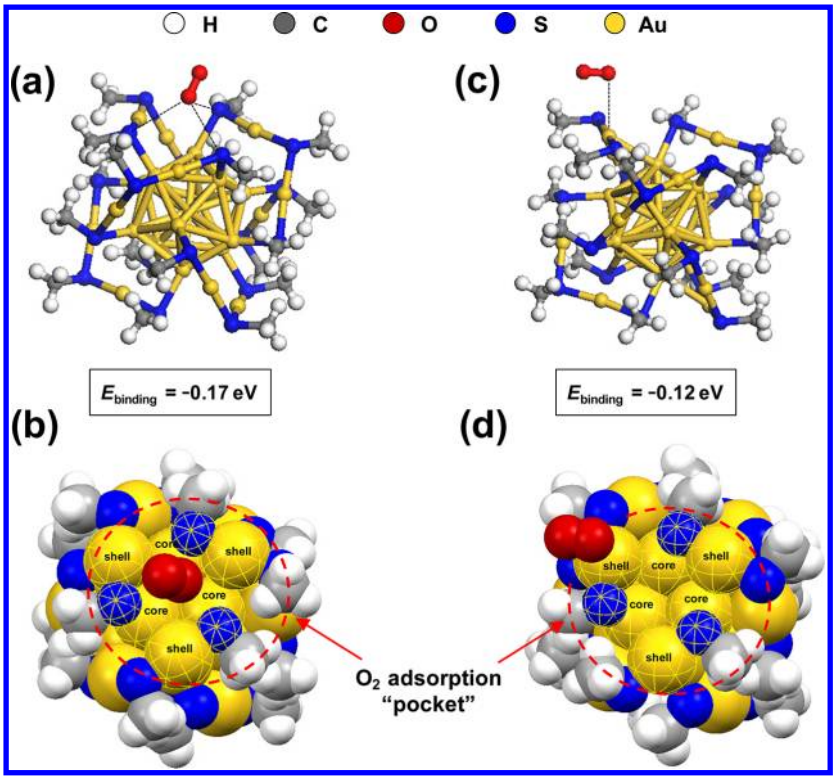

Figure 4. Optimized structures of O_2 adsorbed on $Au_{25}(SCH_3)_{18}^-$ predicted from density functional theory (DFT). Two weakly bound states were identified: (a,b) a three-fold interaction between O_2 and three S atoms in the ligand shell of ground-state $Au_{25}(SCH_3)_{18}^-$ and (c,d) a one-fold interaction between O_2 and a single Au atom in the ligand shell of ground state $Au_{25}(SCH_3)_{18}^-$. The sizes of the Au, S, C, and H atoms in the space-filled models (panels b and d) were adjusted to emphasize the active site adsorption "pocket".

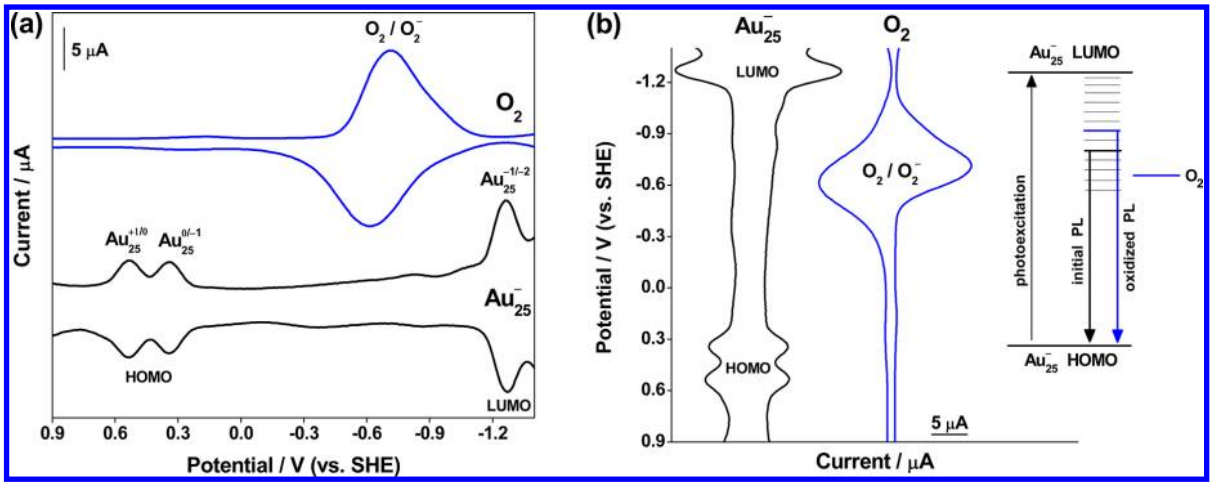

Figure 5. (a) Square-wave voltammograms (SWVs) of Au_{25}^- and O_2 in DMF + 0.1 M tetrabutylammonium perchlorate (TBAP). Curves were collected with a scan rate of 50 mV s^{-1}, the O_2 SWV was scaled by 1/5th for comparison to Au_{25}^-, and potentials were calibrated into the standard hydrogen electrode scale (SHE) using ferrocene (Fc/Fc^+ = 0.7112 V vs SHE in DMF + 0.1 M TBAP).[38] (b) Alternative SWV presentation that quantifies the position of the Au_{25}^- HOMO and LUMO in comparison with the O_2 accepting level (the O_2/O_2^- redox couple). The positions of the Au_{25}^- HOMO and LUMO were taken as the formal potential of the $Au_{25}^{0/-1}$ and $Au_{25}^{-1/-2}$ redox peaks. The positions of emissive midgap states, with respect to the $Au_{25}^{0/-1}$ redox peak (Au_{25}^- HOMO), were taken from the PL spectra in Figure 2a. The position of the O_2 accepting level was taken as the formal potential of the O_2/O_2^- redox peak.

O_2 and *partially* ligand-protected Au_{25}^- clusters.[13] They found that ligand removal activated the cluster and introduced electron density above the HOMO–LUMO gap. After such treatment, stable O_2 binding energies ranged between 0.62 and 0.72 eV (opposite sign convention), and charge was donated into a $2\pi^*$ orbital of O_2. The strong O_2 adsorption produced shorter O–Au bond distances (2.24–2.36 Å) and longer O–O bond distances (1.30–1.31 Å) compared with our results. The contrast between Häkkinen and coworkers' results and our results illustrate the different chemical properties of *partially* ligand-protected versus *fully* ligand-protected cluster models.

Nonaqueous electrochemistry is a powerful complement to optical spectroscopy because it can resolve the redox potentials of molecular energy levels. Figure 5a presents the square-wave

dx.doi.org/10.1021/jz302056q | J. Phys. Chem. Lett. 2013, 4, 195–202

voltammogram (SWV) of Au_{25}^- in N_2-purged DMF with a supporting electrolyte of 0.1 M tetrabutylammonium perchlorate (TBAP). The Au_{25}^- SWV contains several redox peaks that correspond to the HOMO and LUMO. The $Au_{25}^{+1/0}$ and $Au_{25}^{0/-1}$ redox peaks at +0.54 and +0.34 V represent charge injection into the cluster HOMO. The $Au_{25}^{-1/-2}$ redox peak at −1.26 V represents charge injection into the LUMO. A so-called charging energy associated with the electrochemical addition or removal of electrons increases the apparent HOMO−LUMO peak separation and splits the HOMO into two redox peaks.[27,37] The magnitude of the charging energy is typically taken as the HOMO redox peak separation (0.2 V). Murray and coworkers have suggested the Au_{25}^- E_g can be estimated by subtracting the charging energy from the $Au_{25}^{0/-1}$ and $Au_{25}^{-1/-2}$ peak separation.[27] This analysis provides an E_g estimate of 1.40 eV that is consistent with the spectroscopically determined and theoretically predicted values.[1]

Figure 5a also contains the SWV of O_2 in DMF + 0.1 M TBAP, where the one-electron reduction of O_2 into O_2^- occurred at a formal potential of −0.66 V.[39] The formal potential is defined as the average peak potential from the anodic and cathodic scans. Molecular O_2 is reduced into the O_2^- anion in aprotic, nonaqueous solvents like DMF. The O_2 reduction reaction does not proceed further in this solvent−electrolyte system because TBA^+ and other bulky counterions form stable ion pairs with O_2^-, for example, $TBA^+-O_2^-$.[40] This nonaqueous process differs from the multielectron reduction of O_2 into H_2O_2 and H_2O that occurs at roughly +1 V in aqueous solvents.[41]

Figure 5b contains an alternative presentation of the SWVs and an energy level diagram that compares the Au_{25}^- HOMO and LUMO to the O_2 electron-accepting level (O_2/O_2^- redox couple). Here the positions of the Au_{25}^- HOMO and LUMO were taken as the formal potential of the $Au_{25}^{0/-1}$ and $Au_{25}^{-1/-2}$ redox peaks. The positions of emissive midgap states, with respect to the $Au_{25}^{0/-1}$ redox peak (Au_{25}^- HOMO), were taken from the PL spectra in Figure 2a. Finally, the O_2 electron-accepting level was taken as the formal potential of the O_2/O_2^- redox couple.

Figure 5b clearly shows the O_2 electron-accepting level sits within the Au_{25}^- HOMO−LUMO gap. Therefore, O_2 cannot spontaneously extract electrons from the lower lying HOMO of ground-state Au_{25}^-. A similar situation occurs during illumination with low-energy NIR light because electrons are not photoexcited into the Au_{25}^- LUMO. However, if Au_{25}^- is illuminated with sufficiently energetic light, then electrons are photoexcited across the HOMO−LUMO gap and subsequent electron relaxation populates midgap states. Energy overlap between these midgap states and the O_2-accepting level creates a photoaccessible charge-transfer pathway. Sakai and Tatsuma have proposed a similar mechanism to explain the photoelectrochemical behavior of Au_{25}^--decorated TiO_2 electrodes.[42] In their case, Au_{25}^- photoexcitation leads to charge donation into the conduction band of TiO_2.

In situ spectroelectrochemistry was used to benchmark the charge-dependent optical properties of Au_{25}^- and quantify the photomediated electron transfer. This technique is useful because particular Au_{25}^z charge states (z = −1, 0, +1) can be isolated by applying appropriate electrochemical potentials.[27] For example, the application of a potential that is more anodic than the $Au_{25}^{0/-1}$ redox peak at +0.34 V will produce neutral Au_{25}^0. Similarly, the application of a potential that is more anodic than the $Au_{25}^{+1/0}$ redox peak at +0.54 V will produce cationic Au_{25}^+.

Figure 6a contains the in situ spectroelectrochemical modification of Au_{25} charge states in N_2-purged DMF with a supporting electrolyte of 0.1 M TBAP. The absorbance and PL spectra of the initially anionic Au_{25}^- cluster (black curves) were collected in an open circuit configuration without the application of electrochemical potential. The cluster was oxidized into the neutral Au_{25}^0 form by applying a potential of +0.44 V (red curves). It was further oxidized into the cationic Au_{25}^+ form by applying a potential of +0.84 V (blue curves). These spectroscopic assignments are consistent with previous reports of chemical and electrochemical Au_{25}^- oxidation.[27,30,35,36]

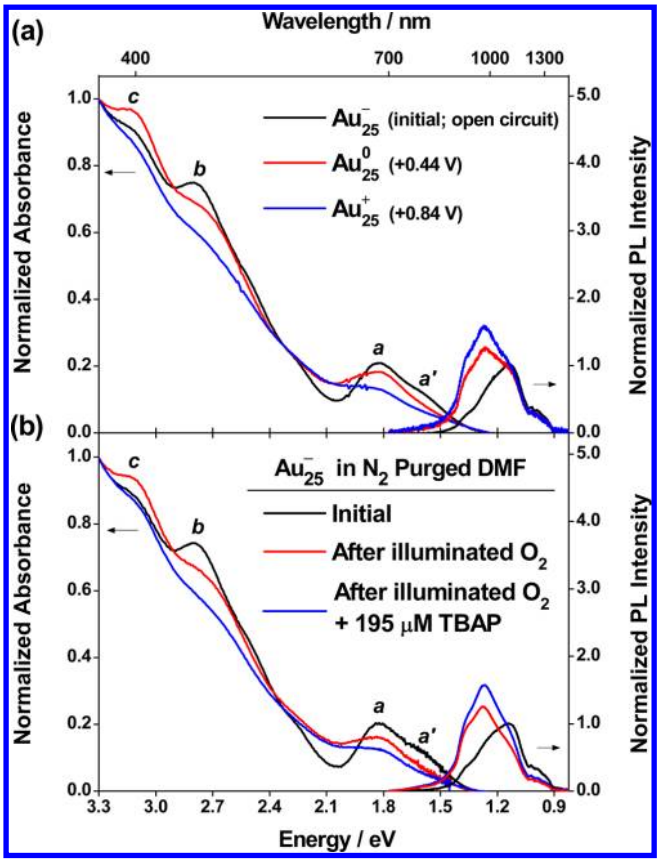

Figure 6. (a) Normalized absorbance and normalized PL spectra of Au_{25}^- + 0.1 M TBAP during in situ electrochemical modification of the charge state. Please see Figure 5a for the position of the applied electrochemical potentials with respect to the Au_{25}^- redox peaks. (b) Normalized absorbance and normalized PL spectra of initially anionic Au_{25}^- in N_2-purged DMF (black curves), after illuminated O_2 exposure (red curves, likely Au_{25}^0 formation), and after illuminated O_2 exposure in the presence of 195 μM TBAP (blue curves, likely Au_{25}^+ formation). Solutions were illuminated with a fiber optic light source through a 3.88 eV low-pass optical filter ($h\nu$ < 3.88 eV, λ > 320 nm). Control experiments ruled out cluster oxidation by TBAP (Figure S15 in the Supporting Information).

The spectroelectrochemical results in Figure 6a allowed us to assign the photomediated oxidation of Au_{25}^- as an inherently one-electron process. For example, Figure 6b contains the absorbance and PL spectra of a N_2 purged Au_{25}^- solution before (black curves) and after (red curves) 1 h of illuminated O_2 exposure; solutions were illuminated with a fiber optic light

dx.doi.org/10.1021/jz302056q | J. Phys. Chem. Lett. 2013, 4, 195−202

source through a 3.88 eV low-pass optical filter (λ > 320 nm). The resulting spectra were consistent with the conversion of the initially anionic Au_{25}^- into the neutral Au_{25}^0 form,[12,27,30,35,36] and we propose that the photomediated Au_{25}^-–O_2 charge transfer produced Au_{25}^0 and O_2^-, as shown in eq 1.

$$Au_{25}^- - TOA^+ + O_2 \xrightarrow{h\nu > E_g} Au_{25}^0 + O_2^- - TOA^+ \quad (1)$$

We hypothesize the 1:1 cluster to counterion ratio-limited photomediated Au_{25}^-–O_2 charge transfer to a one-electron process. The initially anionic Au_{25}^- cluster carried a single TOA^+ counterion (Figure S1 in the Supporting Information). After the cluster was oxidized into neutral Au_{25}^0, it no longer needed a counterion.[12] This left TOA^+ free to stabilize the O_2^- reaction product by forming a TOA^+–O_2^- ion pair.[40] Consumption of the TOA^+ counterion prevented further O_2^- stabilization, and the cluster remained in a neutral Au_{25}^0 charge state. In this regard, the cluster counterion was a limiting reagent.

Further Au_{25}^0–O_2 charge transfer was possible in the presence of excess counterion (in the form of TBAP). TBA^+ is similar to the cluster counterion because both are bulky cations that can stabilize O_2^-.[40] The blue curves in Figure 6b represent a N_2-purged solution of Au_{25}^- + 195 μM TBAP after 1 h of illuminated O_2 exposure ($h\nu$ < 3.88 eV). The Au_{25}^- concentration was estimated to be ~16 μM from the raw absorbance spectrum and the reported molar absorptivity (ε = 8.8×10^3 M^{-1} cm^{-1} at peak *a*).[43] The resulting spectral changes were consistent with the formation of cationic Au_{25}^+, as identified through our spectroelectrochemical experiments and previous literature reports.[27,30,35,36] Control experiments ruled out cluster oxidation by TBAP (Figure S15 in the Supporting Information). Rather, the excess counterion stabilized further O_2^- production and allowed photomediated charge transfer to proceed past a one-electron process. The perchlorate anion component of TBAP likely stabilized the cationic Au_{25}^+ cluster. We hypothesize that unfavorable interaction between cationic Au_{25}^+ and O_2 prevented further charge transfer or oxidative degradation of the cluster. These observations indicate that O_2 can oxidize the cluster past the neutral Au_{25}^0 form so long as the solution is illuminated with sufficiently energetic light *and* excess counterion is present.

We point out that singlet oxygen ($^1O_2$) can be formed during the process of PL quenching[44] and that $^1O_2$ can behave as an oxidizing agent in certain situations.[45] However, the $^1O_2$-accepting level is shifted approximately +1 V with respect to ground-state (triplet) O_2.[46] On the basis of the electrochemical data in Figure 5, this would place the $^1O_2$ accepting level and the $Au_{25}^{0/-1}$ (HOMO) redox peak at nearly identical potentials. As such, and any charge transfer between Au_{25}^- and $^1O_2$ should be reversible,[39] precluding significant $^1O_2$ contribution to the irreversible cluster oxidation observed in this study. We also note that previous reports of Au_{25}^- oxidation with O_2 were accomplished by exposing Au_{25}^- to room air under ambient conditions.[12,30] Exposure to ambient air could potentially affect the O_2 redox potential by introducing water into the system, but we did not find evidence of spontaneous charge transfer between Au_{25}^- and "wet" O_2 in the absence of light (Figure S16 in the Supporting Information). This result indicates that the previous reports of Au_{25}^- oxidation by O_2 were likely photomediated, albeit unrealized at the time.

We tested the generality of our proposed mechanism by investigating the interaction between Au_{25}^- and quinoline. Quinoline is a two-ringed, nitrogen-containing molecule that has an electron-accepting level slightly below the Au_{25}^- LUMO.[47] In accordance with our hypothesis, we observed charge transfer only after Au_{25}^- photoexcitation (Figure S17 and Table S2 in the Supporting Information). This result shows that photomediated charge transfer is not restricted to O_2, and it likely extends to a broad range of molecules with electron-accepting levels in the proximity of the Au_{25}^- LUMO. Finally, we confirmed that spontaneous charge transfer can occur with electron acceptors having levels below the Au_{25}^- HOMO. Experiments with $K_3Fe(CN)_6$ illustrate that spontaneous oxidation of Au_{25}^- occurs with associated spectral changes (Figure S18 in the Supporting Information), and similar spontaneous charge transfer was previously noted between Au_{25}^- and $Ce(SO_4)_2$, Ag^+ and oxoammonium cations,[29,35] and peroxide species.[36] These results further cement the role of the HOMO, LUMO, and excited electronic states in the surface chemistry of atomically precise, ligand-protected Au_{25}^- clusters.

In conclusion, we have shown that light can play an important role in the chemistry of Au_{25}^- clusters. Our experimental and computational findings refine the suspected role of the Au_{25}^- ground state charge. Specifically, we have shown that the Au_{25}^- anionic charge does not play a substantial role in charge transfer with O_2 or quinoline. Rather, HOMO–LUMO energies, photoexcitation, and the relative position of electron-acceptor levels more directly impact Au_{25}^- chemistry. This phenomenon may apply to other ligand-protected clusters of different size, composition, and charge, so long as they have appropriate HOMO–LUMO energies and counterions are available to stabilize reaction products. The identification of such photochemical processes may help develop new cluster-adsorbate models, expand the range of reactions available to these materials, and further our understanding of ligand-protected cluster chemistry.

■ ASSOCIATED CONTENT

Supporting Information

Experimental and computational methods and additional data and analysis. This material is available free of charge via the Internet at http://pubs.acs.org.

■ AUTHOR INFORMATION

Corresponding Author

*E-mail: Douglas.Kauffman@contr.netl.doe.gov.

Notes

The authors declare no competing financial interest.

■ ACKNOWLEDGMENTS

R.J. acknowledges research support by the Air Force Office of Scientific Research under AFOSR award no. FA9550-11-1-9999 (FA9550-11-1-0147). This technical effort was performed in support of ongoing NETL research under RES contract DE-FE0004000. This report was prepared as an account of work sponsored by an agency of the United States Government. Neither the United States Government nor any agency thereof, nor any of their employees, makes any warranty, express or implied, or assumes any legal liability or responsibility for the accuracy, completeness, or usefulness of any information, apparatus, product, or process disclosed, or represents that its use would not infringe privately owned rights. Reference herein

to any specific commercial product, process, or service by trade name, trademark, manufacturer, or otherwise does not necessarily constitute or imply its endorsement, recommendation, or favoring by the United States Government or any agency thereof. The views and opinions of authors expressed herein do not necessarily state or reflect those of the United States Government or any agency thereof.

REFERENCES

(1) Zhu, M.; Aikens, C. M.; Hollander, F. J.; Schatz, G. C.; Jin, R. Correlating the Crystal Structure of a Thiol-Protected Au_{25} Cluster and Optical Properties. *J. Am. Chem. Soc.* **2008**, *130*, 5883−5885.

(2) Heaven, M. W.; Dass, A.; White, P. S.; Holt, K. M.; Murray, R. W. Crystal Structure of the Gold Nanoparticle $[N(C_8H_{17})_4][Au_{25}(SCH_2CH_2Ph)_{18}]$. *J. Am. Chem. Soc.* **2008**, *130*, 3754−3755.

(3) Qian, H.; Zhu, M.; Wu, Z.; Jin, R. Quantum Sized Gold Nanoclusters with Atomic Precision. *Acc. Chem. Res.* **2012**, *45*, 1470−1479.

(4) Parker, J. F.; Fields-Zinna, C. A.; Murray, R. W. The Story of a Monodisperse Gold Nanoparticle: $Au_{25}L_{18}$. *Acc. Chem. Res.* **2010**, *43*, 1289−1296.

(5) Maity, P.; Xie, S.; Yamauchi, M.; Tsukuda, T. Stabilized Gold Clusters: from Isolation Toward Controlled Synthesis. *Nanoscale* **2012**, *4*, 4027−4037.

(6) Zhu, Y.; Qian, H.; Zhu, M.; Jin, R. Thiolate-Protected Au_n Nanoclusters as Catalysts for Selective Oxidation and Hydrogenation Processes. *Adv. Mater.* **2010**, *22*, 1915−1920.

(7) Nie, X.; Qian, H.; Ge, Q.; Xu, H.; Jin, R. CO Oxidation Catalyzed by Oxide-Supported $Au_{25}(SR)_{18}$ Nanoclusters and Identification of Perimeter Sites as Active Centers. *ACS Nano* **2012**, *6*, 6014−6022.

(8) Zhu, Y.; Qian, H.; Drake, B. A.; Jin, R. Atomically Precise $Au_{25}(SR)_{18}$ Nanoparticles as Catalysts for the Selective Hydrogenation of α,β-Unsaturated Ketones and Aldehydes. *Angew. Chem., Int. Ed.* **2010**, *49*, 1295−1298.

(9) Zhu, Y.; Wu, Z.; Gayathri, C.; Qian, H.; Gil, R. R.; Jin, R. Exploring Stereoselectivity of Au_{25} Nanoparticle Catalyst for Hydrogenation of Cyclic Ketone. *J. Catal.* **2010**, *271*, 155−160.

(10) Kauffman, D. R.; Alfonso, D.; Matranga, C.; Qian, H.; Jin, R. Experimental and Computational Investigation of Au_{25} Clusters and CO_2: A Unique Interaction and Enhanced Electrocatalytic Activity. *J. Am. Chem. Soc.* **2012**, *134*, 10237−10243.

(11) Chen, W.; Chen, S. Oxygen Electroreduction Catalyzed by Gold Nanoclusters: Strong Core Size Effects. *Angew. Chem., Int. Ed.* **2009**, *48*, 4386−4389.

(12) Zhu, M.; Eckenhoff, W. T.; Pintauer, T.; Jin, R. Conversion of Anionic $[Au_{25}(SCH_2CH_2Ph)_{18}]^-$ Cluster to Charge Neutral Cluster *via* Air Oxidation. *J. Phys. Chem. C* **2008**, *112*, 14221−14224.

(13) Lopez-Acevedo, O.; Kacprzak, K. A.; Akola, J.; Häkkinen, H. Quantum Size Effects in Ambient CO Oxidation Catalysed by Ligand-Protected Gold Clusters. *Nat. Chem.* **2010**, *2*, 329−334.

(14) Gao, Y.; Shao, N.; Pei, Y.; Chen, Z.; Zeng, X. C. Catalytic Activities of Subnanometer Gold Clusters (Au_{16} − Au_{18}, Au_{20}, and Au_{27} − Au_{35}) for CO Oxidation. *ACS Nano* **2011**, *5*, 7818−7829.

(15) Staykov, A.; Nishimi, T.; Yoshizawa, K.; Ishihara, T. Oxygen Activation on Nanometer-Size Gold Nanoparticles. *J. Phys. Chem. C* **2012**, *116*, 15992−16000.

(16) Liu, Y.; Tsunoyama, H.; Akita, T.; Xie, S.; Tsukuda, T. Aerobic Oxidation of Cyclohexane Catalyzed by Size-Controlled Au Clusters on Hydroxyapatite: Size Effect in the sub-2 nm Regime. *ACS Catal.* **2011**, *1*, 2−6.

(17) Liu, Y.; Tsunoyama, H.; Akita, T.; Tsukuda, T. Efficient and Selective Epoxidation of Styrene with TBHP Catalyzed by Au_{25} Clusters on Hydroxyapatite. *Chem. Commun.* **2010**, *46*, 550−552.

(18) Akola, J.; Walter, M.; Whetten, R. L.; Häkkinen, H.; Grönbeck, K. On the Structure of Thiolate-Protected Au_{25}. *J. Am. Chem. Soc.* **2008**, *130*, 3756−3757.

(19) Negishi, Y.; Chaki, N. K.; Shichibu, Y.; Whetten, R. L.; Tsukuda, T. Origin of the Magic Stability of Thiolated Gold Clusters: A Case Study on $Au_{25}(SC_6H_{13})_{18}$. *J. Am. Chem. Soc.* **2007**, *129*, 11322−11323.

(20) Wu, Z.; Jin, R. Stability of the Two Au-S Binding Modes in $Au_{25}(SG)_{18}$ Nanoclusters Probed by NMR and Optical Spectroscopy. *ACS Nano* **2009**, *3*, 2036−2042.

(21) Shibu, E. S.; Muhammed, M. A. H.; Tsukuda, T.; Pradeep, T. Ligand Exchange of $Au_{25}SG_{18}$ Leading to Functionalized Gold Clusters: Spectroscopy, Kinetics, and Luminescence. *J. Phys. Chem. C* **2008**, *112*, 12168−12176.

(22) Love, J. C.; Estroff, L. A.; Kriebel, J. K.; Nuzzo, R. G.; Whitesides, G. M. Self-Assembled Monolayers of Thiolates on Metals as a Form of Nanotechnology. *Chem. Rev.* **2005**, *105*, 1103−1170.

(23) Zhu, Y.; Qian, H.; Jin, R. Catalysis Opportunities of Atomically Precise Gold Nanoclusters. *J. Mater. Chem.* **2011**, *21*, 6793−6799.

(24) Aikens, C. M. Geometric and Electronic Structure of $Au_{25}(SPhX)_{18}^-$ (X = H, F, Cl, BR, CH_3, OCH_3). *J. Phys. Chem. Lett.* **2010**, *1*, 2594−2599.

(25) Devadas, M. S.; Bairu, S.; Qian, H.; Sinn, E.; Jin, R.; Ramakrishna, G. Temperature-Dependent Optical Absorption Properties of Monolayer-Protected Au_{25} and Au_{38} clusters. *J. Phys. Chem. Lett.* **2011**, *2*, 2752−2758.

(26) Qian, H.; Sfeir, M. Y.; Jin, R. Ultrafast Relaxation Dynamics of $[Au_{25}(SR)_{18}]^q$ Nanoclusters: Effects of Charge State. *J. Phys. Chem. C* **2010**, *114*, 19935−19940.

(27) Lee, D.; Donkers, R. L.; Wang, G.; Harper, A. S.; Murray, R. W. Electrochemistry and Optical Absorbance and Luminescence of Molecule-Like Au_{38} Nanoparticles. *J. Am. Chem. Soc.* **2004**, *126*, 6193−6199.

(28) Wang, G.; Guo, R.; Kalyuzhny, G.; Choi, J.-P.; Murray, R. W. NIR Luminescence Intensities Increase Linearly with Proportion of Polar Thiolate Ligands in Protecting Monolayers of Au_{38} and Au_{140} Quantum dots. *J. Phys. Chem. B* **2006**, *110*, 20282−20289.

(29) Choi, J.-P.; Fields-Zinna, C. A.; Stiles, R. L.; Balasubramanian, R.; Dougals, A. D.; Crowe, M. C.; Murray, R. W. Reactivity of $[Au_{25}(SCH_2CH_2Ph)_{18}]^{1-}$ Nanoparticles with Metal Ions. *J. Phys. Chem. C* **2010**, *114*, 15890−15896.

(30) Wu, Z.; Jin, R. On the Ligand's Role in the Fluorescence of Gold Nanoclusters. *Nano Lett.* **2010**, *10*, 2568−2573.

(31) Swanick, K. N.; Hesari, M.; Workentin, M. S.; Ding, Z. Interrogating Near-Infrared Electrogenerated Chemiluminescence of $Au_{25}(SC_2H_4Ph)_{18}^+$ Clusters. *J. Am. Chem. Soc.* **2012**, *134*, 15205−15208.

(32) Devadas, M. S.; Kim, J.; Sinn, E.; Lee, D.; Goodson, T.; Ramakrishna, G. Unique Ultrafast Visible Luminescence in Monolayer-Protected Au_{25} Clusters. *J. Phys. Chem. C* **2010**, *114*, 22417−22423.

(33) Wen, X.; Yu, P.; Toh, Y.-R.; Hsu, A.-C.; Lee, Y.-C.; Tang, J. Fluorescence Dynamics in BSA-Protected Au_{25} Nanoclusters. *J. Phys. Chem. C* **2012**, *116*, 19032−19038.

(34) Negishi, Y.; Iwai, T.; Ide, M. Continuous Modulation of Electronic Structure of Stable Thiolate-Protected Au_{25} Cluster by Ag Doping. *Chem. Commun.* **2010**, *46*, 4713−4715.

(35) Liu, Z.; Zhu, M.; Meng, X.; Xu, G.; Jin, R. Electron Transfer Between $[Au_{25}(SC_2H_4Ph)_{18}]^-TOA^+$ and Oxoammonium Cations. *J. Phys. Chem. Lett.* **2011**, *2*, 2104−2109.

(36) Venzo, A.; Antonello, S.; Gascón, J. A.; Guryanov, I.; Leapman, R. D.; Perera, N. V.; Sousa, A.; Zamuner, M.; Zanella, A.; Maran, F. Effect of the Charge State (z = −1, 0, +1) on the Nuclear Magnetic Resonance of Monodisperse $Au_{25}[S(CH_2)_2Ph]_{18}^z$ Clusters. *Anal. Chem.* **2011**, *83*, 6355−6362.

(37) Franceschetti, A.; Zunger, A. Pseudopotential Calculations of Electron and Hole Addition Spectra of InAS, InP, and Si Quantum Dots. *Phys. Rev. B* **2000**, *62*, 2614−2623.

(38) Connelly, N. G.; Geiger, W. E. Chemical Redox Agents for Organometallic Chemistry. *Chem. Rev.* **1996**, *96*, 877−910.

(39) Bard, A. J.; Faulkner, L. R. *Electrochemical Methods: Fundamentals and Applications*, 2nd ed.; John Wiley & Sons: New York, 2001.

(40) Laoire, C. O.; Mukerjee, S.; Abraham, K. M.; Plichta, E. J.; Hendrickson, M. A. Influence of Nonaqueous Solvents on the Electrochemistry of Oxygen in the Rechargeable Lithium-Air Battery. *J. Phys. Chem. C* **2010**, *114*, 9178−9186.
(41) Marković, N. M.; Schmidt, T. J.; Stamenković, V.; Ross, P. N. Oxygen Reduction Reaction on Pt and Pt Bimetallic Surfaces: A Selective Review. *Fuel Cells* **2001**, *1*, 105−116.
(42) Sakai, N.; Tatsuma, T. Photovoltaic Properties of Glutathione-Protected Gold Clusters Adsorbed on TiO_2 Electrodes. *Adv. Mater.* **2010**, *22*, 3185−3188.
(43) Negishi, Y.; Nobusada, K.; Tsukuda, T. Glutathione-Protected Gold Clusters Revisited: Bridging the Gap between Gold(I)−Thiolate Complexes and Thiolate-Protected Gold Nanocrystals. *J. Am. Chem. Soc.* **2005**, *127*, 5261−5270.
(44) Wilkinson, F. Quenching of Electronically Excited States by Molecular Oxygen. *Pure Appl. Chem.* **1997**, *69*, 851−856.
(45) DeRosa, M. C.; Crutchley, R. J. Photosensitized Singlet Oxygen and its Applications. *Coord. Chem. Rev.* **2002**, *233*−*234*, 351−371.
(46) Ijeri, V. S.; Daasbjerg, K.; Ogilby, P. R.; Poulsen, L. Spacial and Temporal Electrochemical Control of Singlet Oxygen Production and Decay in Photosensitized Experiments. *Langmuir* **2008**, *24*, 1070−1079.
(47) Smith, W. H.; Bard, A. J. Electrochemical Reactions of Organic Compounds in Liquid Ammonia. III. Reductive Alkylation of Quinoline. *J. Am. Chem. Soc.* **1975**, *97*, 6491−6495.